Photodetachment of H^- in a Strong Infrared Laser Field

Rainer Reichle, Hanspeter Helm, and Igor Yu. Kiyan
Fakultät für Physik, Albert-Ludwigs-Universität, D-79104 Freiburg, Germany
(Received 20 March 2001; published 26 November 2001)

Negative hydrogen ions are exposed to a short infrared laser pulse of 2.15 μm wavelength and 250 fs duration. An imaging technique is used to record the energy resolved angular distribution of photoelectrons. The energy spectrum reveals at least three excess photon detachment channels. A quantum interference effect, resulting in an unusual dependence of the angular distribution on the electron kinetic energy, is most prominent in the lowest two-photon detachment channel. The appearance of this effect is discussed in terms of the threshold law of photodetachment.

DOI: 10.1103/PhysRevLett.87.243001 PACS numbers: 32.80.Gc, 32.80.Rm

The phenomenon of electron ionization from an atomic system in a strong laser field received much attention over the past years. Phenomena, such as above threshold ionization (ATI), tunnel ionization, and multiple ionization of atoms were observed and characterized [1]. Various nonperturbative theoretical methods were developed to describe these processes. One of them, the Keldysh-Faisal-Reiss (KFR) theory, treats the problem analytically [2]. This theory was developed to describe ionization from an atomic system with a short-range potential. Negative ions represent such a system and, thus, the KFR approach is particularly appropriate for the description of photodetachment. However, most of the strong field experiments to date were performed on neutral atoms, where the long range Coulomb potential needs to be taken into account, and comprehensive experimental verification of the KFR theory is missing so far.

The analytical approach makes the KFR theory powerful to describe quantitatively effects of ionization in a strong laser field. In this context a new effect was recently predicted and described in terms of quantum interference of classical electron trajectories [3,4]. The interference leads to a specific dependence of angular and energy distributions of photoelectrons on the laser intensity, discussed in two recent experiments [5,6] on photoionization of noble gases. In this Letter we report on the first observation of this interference effect in a negative ion. The different appearance of this effect in the case of photodetachment is due to a fundamentally different threshold law which governs the process at low photoelectron energies.

The main difficulty of experiments on photodetachment in a strong laser field is the depletion of negative ions by a low order detachment process at the leading front of laser pulse, where the intensity is already sufficient to drive the detachment step. The first observation of excess photon detachment (EPD), the analog to ATI, was reported in the F^-, Cl^-, and Au^- negative ions [7–9], which have a relatively high binding energy of the outer electron. The lowest order detachment process required absorption of two or more photons in these experiments. It is not surprising that EPD photoelectron spectra were more prominent in these earlier experiments than in later experiments on H^- [10,11], where only the first EPD channel was observed in the presence of the prevailing one-photon detachment process. Despite the rather high peak laser intensity in the latter observations, the EPD signal was very low because of saturation of the one-photon process. One should also mention a recent experiment [12] where photodetachment of H^- was studied at the threshold of the one-photon process. Here the two-photon channel was observed due to the fact that in negative ions, according to the Wigner threshold law [13], the probability of photodetachment tends to zero at threshold, thus, effectively suppressing the one-photon channel. Higher EPD channels were not observed in this experiment due to saturation of the two-photon process. Reducing the interaction time of negative ions with the laser beam and increasing the order of the lowest channel is a solution to overcome the depletion problem. In the present experiment we investigate angle resolved energy distributions of photoelectrons produced by photodetachment of H^- in a laser pulse of 250 fs duration and 2.15 μm wavelength. The infrared wavelength requires absorption of at least two photons in order to overcome the binding energy of 0.754 21 eV of H^-. Under these conditions, we observe a photoelectron spectrum which reveals at least three prominent EPD channels. An analysis of angular distributions will be given, showing that the predicted [3] quantum interference effect is most pronounced near the threshold of photodetachment.

In our experiment, negative ions of H^- are extracted from a hollow cathode plasma source and accelerated to a kinetic energy of 3 keV. The 100 nA ion beam is mass selected in a Wien filter and delivered into the detection chamber by bending the beam by 90° in a quadrupole deflector. Differential pumping allows us to maintain the interaction region at 10^{-10} mbar during the experiment. An electron imaging spectrometer (EIS) is used to detect photoelectrons formed in photodetachment. The ion beam is pulsed synchronously with the laser (10 μs on, 990 μs off) to reduce the background from collisions of negative

ions with residual gas atoms and surfaces of the EIS. At the laser focus, the ion beam is focused to a spot of about 400 μm diameter.

Figure 1 shows schematically the current EIS design. A static electric field is created with a set of electrodes to project photoelectrons onto a pair of microchannel plates with a phosphor screen mounted behind. An electron from a single event gives rise to a light pulse on the phosphor screen at the position where it arrives to the detector. A charge-coupled-device (CCD) camera records pulses appearing during its exposure time, and a frame grabber stores coordinates and intensities of the pixels. Thousands of frames are added to obtain a statistically significant image, which represents an angle resolved momentum distribution of photoelectrons. In order to reduce broadening due to the finite size of the interaction region, the spectrometer is operating in a velocity mapping regime [14], designed to compensate the motion of the target ion.

Our laser system consists of an optical parametric amplifier (OPA) pumped with a mode-locked Ti:sapphire laser at 1 kHz repetition rate. The OPA is operating at the wavelength of 2.15 μm with an averaged output of 56 μJ per pulse. The infrared beam is linearly polarized. It is focused with a lens of 15 cm focal length and intersects the ion beam at 90°, while the polarization is kept parallel to the detector plane. The intensity distribution in the laser focus is measured by scanning a razor blade across the focus. The focus can be well reproduced by a Gaussian shape with a waist of 50 μm (FWHM) and a Rayleigh range of 2 mm. The pulse length is measured with an autocorrelator by producing the fourth harmonic in a BBO crystal. The FWHM of the pulse is 250 fs. The peak intensity in the laser focus is on the order of 1.7×10^{13} W/cm^2. Figure 2 shows accumulated data obtained after a few hours of acquisition (corresponding to $\sim 10^8$ detected electrons).

For a given kinetic energy of photoelectrons, the size of the spatial electron distribution in the detector plane is given by the product of the corresponding electron momentum and projection time. Thus, the detector scale can be expressed in terms of the momentum scale of photoelectrons. In order to calibrate the momentum scale, separate measurements were performed with photoelectrons produced by one-photon detachment in a weak field at three laser wavelengths: 795.5, 590.1, and 397.8 nm. The corresponding kinetic energies of photoelectrons cover the range from 0.804 to 2.363 eV. We found the momentum scale of the detector to be linear with a velocity calibration coefficient of $0.976(3) \times 10^6$ cm/s per 1 pixel of the CCD camera. The resolution is determined by the detector response to a single event. It can be described by a Voigt response function with a FWHM of 7.5 pixels. The response function is used for deconvolution of the data.

The image processing involves an Abel inversion [15], which recovers a 3D distribution of photoelectrons before they are projected onto the detector plane. Assuming axial symmetry with respect to the laser polarization axis, it transforms the distribution of photoelectrons in the (x, y) plane of the detector into a distribution over spherical coordinates (r, θ). The radius r is a measure of the electron velocity, and θ is the polar angle with respect to the laser polarization axis. Using the calibration coefficient defined above, the radial coordinate is converted to the momentum scale and energy scale E of photoelectrons. Figure 3 shows the (E, θ) distribution of photoelectrons obtained from the raw data in Fig. 2. At least three EPD peaks are present in the spectrum. An angle integrated energy spectrum is shown in Fig. 4.

The ponderomotive shift of the peaks increases with the order of EPD channel. This shift, however, is much smaller than the value 7.4 eV, which corresponds to the peak intensity measured in the laser focus. In order to describe the shape of the energy spectrum, one has to take into account the spatial and temporal distribution of the laser intensity, as well as the depletion of negative ions by photodetachment. The ponderomotive acceleration from the laser focus can, however, be neglected, because the short pulse regime is used here. Following the results of Ref. [16], we estimate the acceleration energy to be less than 1 μeV over the

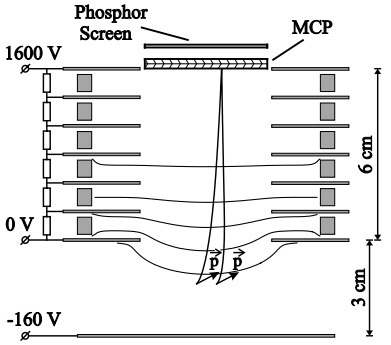

FIG. 1. The EIS design. The interaction region is in the center between two bottom electrodes. A nonuniform electric field creates an electrostatic lens, which projects electrons of the same momentum vector **p** into a single spot on the position sensitive detector. A few simulated equipotential curves and electron trajectories are shown.

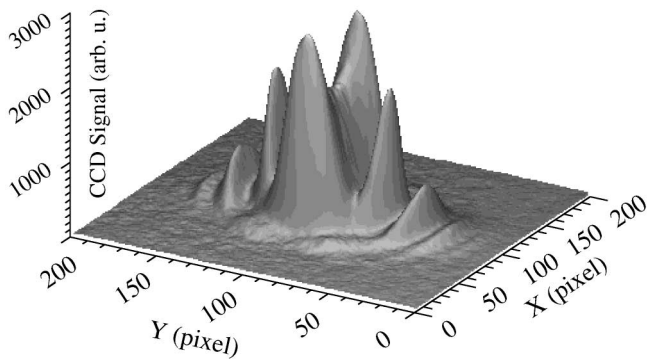

FIG. 2. A raw image of photoelectrons recorded with the CCD camera. The pixel size is equal to 17 μm.

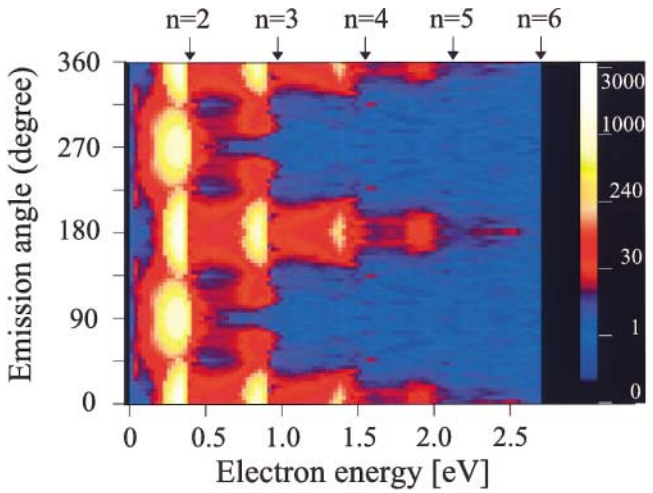

FIG. 3 (color). The (E, θ) distribution of photoelectrons. Energy peaks are broadened and shifted due to the ponderomotive effect. Arrows on the top indicate their unshifted positions [18].

entire energy spectrum, which is much less than the EIS resolution. Using Eq. (33) of Ref. [3] for the photodetachment rate, we reproduced the electron energy distribution by integrating the probability over the volume of the laser focus and the laser pulse duration. Experimental parameters obtained from the laser beam diagnostic were used in this calculation, and the ion depletion was taken into account. The result is normalized to the energy integrated electron signal and is compared to the experimental data in Fig. 4. The theoretical curve reproduces the heights and energy positions of peaks well, though the experimental peaks are slightly narrower and lower for higher EPD channels. It is not excluded that some errors are introduced in the calculation by uncertain experimental parameters. We found, for example, that the theoretical result is dependent on the temporal envelope used to describe the laser pulse. We assumed that this envelope has a sech^2 shape consistent with the autocorrelation trace. However, a slightly different shape might remove the small discrepancy between the experimental and theoretical results.

In the following we discuss the observed energy dependence of the angular distribution (AD). We see from Fig. 3 that the AD of a given n-photon channel is changing as the ponderomotive shift increases. By using the energy position of the photoelectrons as a measure of the ponderomotive shift, $U_p = E_n - E$, an intensity value of $I = 4\omega^2 U_p$ (in atomic units) can be unambiguously defined for electrons of a given energy E produced in the corresponding n-photon process. Here E_n represents the unperturbed kinetic energy, $E_n = n\hbar\omega - 0.754\,21$ eV. Thus, energy resolved ADs do not suffer from the volume effect or from the problem of saturation. It makes ADs for a given intensity and n value the most favorable quantity for comparison of experimental results with a theory.

The lowest (two-photon) detachment channel exhibits a most dramatic change in ADs with increasing laser intensity. This is illustrated in Fig. 5, where two distributions are shown at the intensities corresponding to a ponderomotive shift of 0.1ω and 0.5ω, respectively (that is, 1.3×10^{11} and 6.5×10^{11} W/cm^2). The corresponding kinetic energies are marked as a and b in Fig. 4. The distribution at the lower intensity can be described by a superposition of s and d waves with their relative phase taken into account. Their relative contributions are $(11 \pm 1)\%$ and $(89 \pm 1)\%$, respectively. The perturbation theory [17] produces values of 13% and 87%, respectively, which are close to the experimental results. At the higher intensity, the distribution has an unusual shape with a maximum pointing *perpendicular* to the laser polarization. The

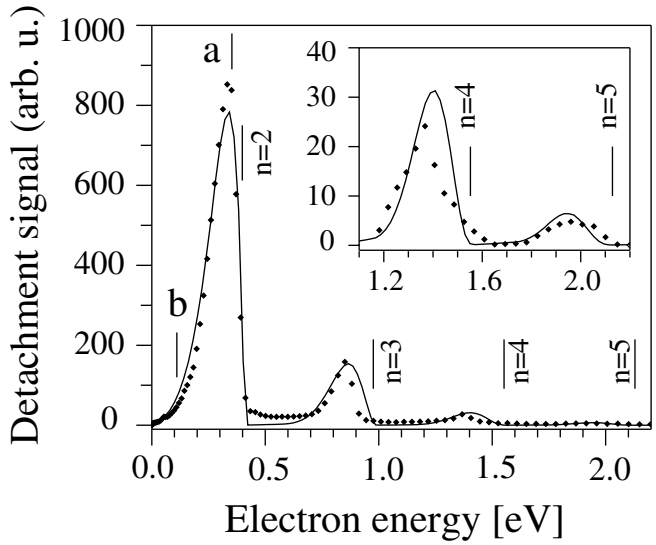

FIG. 4. The energy spectrum integrated over the angle θ: dots—experimental data; solid curve—theoretical results. Angular distributions at energies labeled a and b are shown in Fig. 5. The inset shows higher energy peaks in a greater detail.

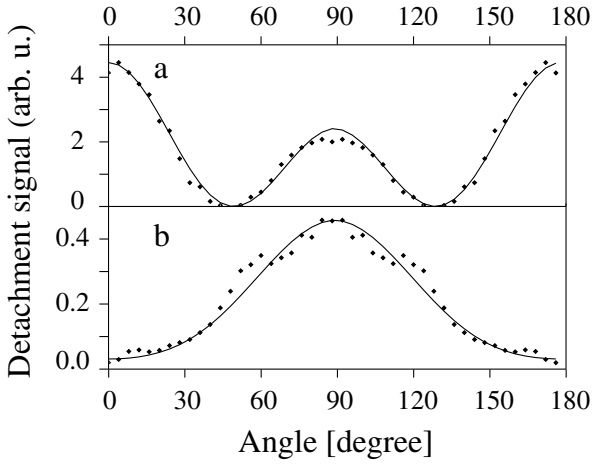

FIG. 5. Angular distributions of photoelectrons in the lowest two-photon detachment channel at two different laser intensities: (a) $I = 1.3 \times 10^{11}$ W/cm^2, (b) $I = 6.5 \times 10^{11}$ W/cm^2. Experimental data (dots) and theoretical results (solid curves) are normalized to each other.

Keldysh-like theory [3] describes such a behavior in terms of quantum interference of electron trajectories. An electron can tunnel into the continuum at different times within a period of the field oscillation. The corresponding continuum wave functions carry the phase of the field at which the electron is emitted. A superposition of wave functions gives rise to the interference effect. The solid lines in Fig. 5, directly calculated using Eq. (33) of Ref. [3], show that the Keldysh-like theory describes the ADs very well.

The higher detachment channels also exhibit modifications of ADs with intensity. This effect, however, is less pronounced as the kinetic energy increases. The presence of the threshold definitely plays an important role in the oscillating behavior of ADs. The effect of modification of ADs can also be understood as being due to higher order processes involving reemission of photons. One should recall at this point that photodetachment at low E is determined by the Wigner threshold law [13]. This law has a general character for a short-range potential system, and it predicts the probability of a reaction near threshold to be proportional to $E^{\ell+1/2}$, where ℓ is the angular momentum of the outgoing electron. Thus, despite a variety of higher order processes, photodetachment at threshold is always determined by the lowest angular momentum available for the outgoing electron. Relative contributions of higher angular momenta decrease dramatically at low E. As a result, ADs undergo a stronger modification in the region close to threshold.

In order to demonstrate the threshold effect, we discuss again the two-photon detachment channel. We fit the ADs at different kinetic energies between zero and $E_{n=2}$ to a superposition of spherical waves with relative phases taken into account. In this energy range we found that only the s and d waves contribute to the fit, although we allowed for higher ℓ values. This finding is consistent with the Wigner law: the population of higher ℓ values by reemission of photons is suppressed because of the ponderomotive closure of the two-photon channel. The ratio of s and d amplitudes versus the energy is shown in Fig. 6. This dependence does not deviate from a linear function by more than 10% in the region up to approximately 160 meV above the threshold, consistent with the Wigner law. At higher energies, there is a strong deviation from the linear dependence. The relative phase between the s and d waves varies monotonically from zero at zero kinetic energy to 0.86 rad at $E_{n=2}$. The solid curve in Fig. 6 represents results obtained from analysis of Eq. (33) of Ref. [3]. The Keldysh-like theory does reproduce the Wigner law at low kinetic energies. This is due to the fact that both theories are developed for an atomic system of a short-range potential.

In conclusion, our experimental verification of the KFR theory shows that it describes well the process of photodetachment. The predicted effect of quantum interference of electron trajectories is observed in energy resolved angular distributions. It is found that the oscillatory behavior of angular distributions is most pronounced near the threshold, where photodetachment is determined by the Wigner threshold law. The Wigner law is a specific feature of a short-range potential, which makes a fundamental difference between photodetachment and photoionization. Further investigations of the role of the threshold law are required. In particular, investigation of the photodetachment process at higher laser intensities, where a closure of channels is realized, represents an interesting task.

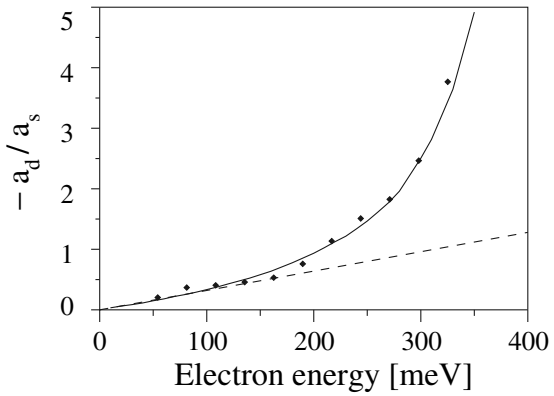

FIG. 6. The amplitude ratio of the d and s waves near the threshold of photodetachment. Dots—experimental results; solid curve—theoretical prediction. Notice that the amplitudes have opposite signs. The dashed line shows the linear dependence according to the Wigner threshold law.

Technical assistance of U. Person and I. Siegel is greatly appreciated. This research has been supported by the Deutsche Forschungsgemeinschaft (SFB 276, TPC 14).

[1] See, e.g., N. B. Delone and V. P. Krainov, *Multiphoton Processes in Atoms* (Springer-Verlag, Berlin, 1994).
[2] L. V. Keldysh, Zh. Eksp. Teor. Fiz. **47**, 1945 (1964) [Sov. Phys. JETP **20**, 1307 (1964)]; F. H. M. Faisal, J. Phys. B **6**, L89 (1973); H. R. Reiss, Phys. Rev. A **22**, 1786 (1980).
[3] G. F. Gribakin and M. Yu. Kuchiev, Phys. Rev. A **55**, 3760 (1997).
[4] R. Kopold *et al.,* Phys. Rev. Lett. **84**, 3831 (2000).
[5] G. G. Paulus *et al.,* Phys. Rev. Lett. **80**, 484 (1998).
[6] G. G. Paulus *et al.,* Phys. Rev. Lett. **84**, 3791 (2000).
[7] C. Blondel *et al.,* J. Phys. B **24**, 3575 (1991).
[8] M. D. Davidson *et al.,* Phys. Rev. Lett. **67**, 1712 (1991); M. D. Davidson *et al.,* Phys. Rev. Lett. **69**, 3459 (1992).
[9] H. Stapelfeldt *et al.,* Phys. Rev. Lett. **67**, 1731 (1991).
[10] A. Stintz *et al.,* Phys. Rev. Lett. **75**, 2924 (1995).
[11] X. M. Zhao *et al.,* Phys. Rev. Lett. **78**, 1656 (1997).
[12] L. Præstegaard *et al.,* Phys. Rev. A **59**, R3154 (1999).
[13] E. P. Wigner, Phys. Rev. **73**, 1002 (1948).
[14] R. Reichle *et al.* (to be published).
[15] C. Bordas *et al.,* Rev. Sci. Instrum. **67**, 2257 (1996).
[16] M. Saeed *et al.,* Phys. Rev. A **49**, 1491 (1994).
[17] L. A. A. Nikolopoulos and P. Lambropoulos, Phys. Rev. A **56**, 3106 (1997).
[18] For a better resolution figure, see our Web page frhewww.physik.uni-freiburg.de/nip/.